Triplet Photophysics of Gold(III) Porphyrins

Mattias P. Eng, Thomas Ljungdahl, Joakim Andréasson,† Jerker Mårtensson, and Bo Albinsson*

Department of Chemistry and Bioscience, Chalmers University of Technology, SE-412 96 Göteborg, Sweden

Received: November 5, 2004

Gold porphyrins are often used as electron-accepting chromophores in donor−acceptor complexes for the study of photoinduced electron transfer, and they can also be involved in triplet−triplet energy-transfer interactions with other chromophores. Since the lowest excited singlet state is very short-lived (240 fs), the triplet state is usually the starting point for the transfer reactions, and it is therefore crucial to understand its photophysics. The triplet state of various gold porphyrins has been reported to have a lifetime of around 1.5 ns at room temperature and to have a biexponential decay both in emission and in transient absorption with decay times of around 10 and 100 μs at 80 K. In this paper, the triplet photophysics of two gold porphyrins (Au^{III} 5,15-bis(3,5-di-*tert*-butylphenyl)-2,8,12,18-tetraethyl-3,7,13,17-tetramethylporphyrin and Au^{III} 5,10,-15,20-tetra(3,5-di-*tert*-butylphenyl)porphyrin) are studied by steady-state and time-resolved absorption and emission spectroscopy over a wide temperature range (4−300 K). The study reveals the existence of a dark state with an approximate lifetime of 50 ns, which was not previously observed. This state acts as an intermediate between the short-lived singlet and the triplet state manifold. In addition, we present DFT calculations, in which the core electrons of the central metal were replaced by a pseudopotential to account for the relativistic effects, which suggest that the lowest excited singlet state is an optically forbidden ligand-to-metal charge-transfer (LMCT) state. This LMCT state is an obvious candidate for the experimentally observed dark state, and it is shown to dictate the photophysical properties of gold porphyrins by acting as a gate for triplet state formation versus direct return to the ground state.

Introduction

The study of porphyrins and porphyrin-related compounds has grown into an extensive research area largely due to their presence in systems involved in natural photosynthesis, where chlorophylls absorb and shuttle energy to a reaction center.[1] Porphyrins are often used instead of chlorophylls in model systems designed to mimic the structures involved in the transfer processes of photosynthesis. Studies using such model systems have involved electron- and excitation energy-transfer reactions[2−22] as well as photoinduced redox reactions as a means to store light energy.[23] The model systems often consist of two moieties, acceptor and donor of the energy and/or electrons, kept at a fixed distance from each other by a spatial separator that either mediates the transfer reactions or not. In some systems, gold(III) porphyrins have been used due to their good stability[24] and suitable redox properties,[4,8,9,25,26] making them excellent as electron acceptors in electron-transfer reactions. The gold(III) porphyrins can act as electron acceptors either in the ground state or in the first excited triplet state (electron hole donor). To quantitatively analyze the photoinduced electron or energy-transfer processes that emanate from the triplet excited gold(III) porphyrins, the intrinsic triplet relaxation processes must be thoroughly understood.

It was observed early on that luminescence from excited gold(III) tetraphenylporphyrin decays biexponentially on the microsecond time scale in organic glasses at 80 K.[27] This behavior has been suggested to originate from slow relaxation between triplet sublevels,[27] different conformations frozen in the rigid media,[10] or the presence of two different ion pairs.[13] In previous studies of gold(III) porphyrins, it has also been tentatively suggested that the short lifetime at room temperature might be due to thermal population of a dark state situated between S_1 and T_1,[28] and there have also been discussions concerning the existence of charge-transfer states.[27,29] Observations of weakly resolved charge-transfer (CT) bands in the absorption spectrum have also been reported,[27,28] and there have been discussions on whether the first reduction takes place at the porphyrin ring[8,28] or at the metal.[25,26] In measurements on a gold(III) 5,15-diphenylporphyrin, it was observed that in addition to the two previously reported microsecond lifetimes the compound also exhibited a lifetime on the nanosecond time scale.[22] This raises interesting questions about the complex photophysics of this class of porphyrin chromophores that might have important implications on their use in donor−acceptor complexes.

In this work, the deactivation of the excited triplet state of gold porphyrins with a varying substitution pattern, Au^{III} 5,15-bis(3,5-di-*tert*-butylphenyl)-2,8,12,18-tetraethyl-3,7,13,17-tetramethylporphyrin (AuP), Au^{III} 5,10,15,20-tetra(3,5-di-*tert*-butylphenyl)-porphyrin (AuT(DtBP)P), and Au^{III} 2,3,7,8,12,13,17,18-octaethylporphyrin (AuOEP) has been studied (Figure 1). The study is closely related to ongoing projects in which photoinduced transfer of electrons and excitation energy between zinc porphyrin and AuP separated by various rigid spacers is investigated.[20,22] As mentioned earlier, a prerequisite for understanding the influence of the transfer reactions on the deactivation of the gold porphyrin triplet state in such model systems is that the intrinsic deactivation of the gold porphyrin

* To whom correspondence should be addressed. Phone: +46317723044. Fax: +46317723858. E-mail: balb@chembio.chalmers.se.

† Current address: Department of Chemistry and Biochemistry, Arizona State University, Tempe, AZ 85287.

10.1021/jp0449399 CCC: $30.25
Published on Web 02/15/2005

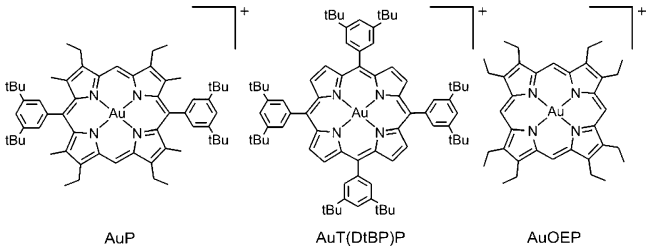

Figure 1. Gold(III) porphyrins used in this study.

monomer is thoroughly characterized. To this end, time-resolved as well as steady-state emission and absorption spectroscopy measurements were performed on the three porphyrins in different media and at temperatures between 4 and 300 K.

Materials and Methods

Materials. The synthesis and purification of $AuP^+BF_4^-$ is described elsewhere.[30] $AuOEP^+BF_4^-$ was prepared by gold insertion into purchased OEP (Aldrich) using the procedure developed by Sauvage et al.[31] $AuT(DtBP)P^+BF_4^-$ was made from $AuT(DtBP)P^+AuCl_4^-$ by ion exchange with 10 equiv of $AgBF_4$ in dichloromethane. $AuT(DtBP)P^+AuCl_4^-$ was synthesized from the free base porphyrin T(DtBP)P according to literature procedures.[32] T(DtBP)P was synthesized from 3,5-di-*tert*-butylbenzaldehyde[33] and pyrrole using the reaction conditions for porphyrin synthesis described by Lindsey et al.[34] All H^1 NMR data were in accordance with those reported in the literature, although $AuOEP^+BF_4^-$ showed some contaminants in the aliphatic region. This should however be of negligible importance to the determination of absorption and emission maxima in the UV−vis region.

Solvents. The solvents ethanol (Kemethyl), diethyl ether (Sigma-Aldrich), isopentane (Merck), toluene (Merck), and methyl cyclohexane (Fluka) were used directly as delivered. The 2-methyl tetrahydrofuran (2-MTHF) (Merck) and methyl methacrylate (MMA) (Merck) were distilled prior to use to remove stabilizers.

To minimize the variations in viscosity and inhibit bimolecular quenching in the whole temperature interval and to get samples more easily handled at low temperatures, the porphyrin samples were immobilized in a solid matrix of poly(methyl methacrylate) (PMMA). The PMMA immobilization was performed by dissolving the porphyrin sample in a glass test tube containing the distilled methyl methacrylate monomer. A minute amount of the initiator azobisisobutyronitrile (AIBN) was added, and the tube was submerged in a water bath with a temperature of 80 °C for approximately 24 h. Subsequently, the glass tube was shattered, and the PMMA "rod" was cut and polished into a square 1 cm × 1 cm rod, mimicking the dimensions of a regular sample cell. The absorption spectra of the rods were compared to those of the respective unpolymerized samples to ensure that no degradation had taken place during the process. At low temperatures, measurements were also performed on samples in a diethyl ether/isopentane/ethanol (5:5:2) (EPA) glass.

Absorption spectra were recorded at room temperature using a normal 1 cm quartz sample cells in a Cary 4B UV−vis spectrophotometer. A baseline of the pure solvent was also recorded for every spectrum. For the steady-state emission measurements, a SPEX Fluorolog-3 spectrofluorimeter was used, and for the time-gated phosphorescence measurements the same setup was used but with a pulsed xenon lamp as the excitation source and a SPEX 1934D3 phosphorimeter as a time-gated detector. Low-temperature measurements were performed using either a temperature-controlled liquid nitrogen cryostat (Oxford LN_2) or, for temperatures below 77 K, a liquid helium cryostat (Oxford Optistat).

The nanosecond to microsecond transient absorption measurements were performed on a setup described previously[21] where the exciting light was provided by a pulsed Nd:YAG laser (Continuum Surelite II-10, pulse width < 7 ns) pumping an OPO, giving a tunable light source in the wavelength region between 400 and 700 nm. Alternatively, the frequency-doubled fundamental output of the laser system (λ = 532 nm) was used. The intensity of the exciting laser was kept below 20 mJ/pulse to prevent photodegradation of the samples. The probe light, penetrating the sample at an angle of 90° relative to the excitation light, was provided by a xenon arc lamp. After passing through the sample, the probe light was passed through a monochromator (symmetrical Czerny−Turner arrangement) and detected by a five-stage Hamamatsu R928 photomultiplier tube. In general, 16−64 transient signals were collected and averaged by a 200 MHz digital oscilloscope (Tektronix TDS2200 2 Gs/s) and stored by a homemade LabView program controlling the whole system.

The picosecond transient absorption measurements were performed using the pump−probe technique on a setup described previously[21] with some modifications on the probe and detector part. In short, the sample was excited at 522 nm with the second harmonic of the signal from a TOPAS OPA (Light Conversion Ltd.). The TOPAS was pumped by a Ti:sapphire regenerative amplifier (Spitfire, Spectra Physics) at 1 kHz repetition rate. The amplifier was in turn pumped by a frequency-doubled diode-pumped Nd:YLF laser (Evolution-X, Spectra Physics) and seeded by a mode-locked femtosecond Ti:sapphire laser (Tsunami, Spectra Physics). The seed laser was pumped by a continuous-wave frequency-doubled diode-pumped Nd:YVO_4 laser (Millennia Vs, Spectra Physics). The output of the amplifier was split in two parts by a beam splitter (70/30) and used as the pump and the probe light, respectively. Instead of the previously described photodiode/monochromator setup, a CCD spectrograph (Avantes) was used, and a white light continuum, for use as the probe light, was generated by letting the probe beam pass through a slowly rotating 4 mm thick CaF_2 disk (Harrick). The samples were kept in continuously moving 2 mm quarts cuvettes. The absorption was approximately 1 at the excitation wavelength (522 nm), and the pulse energy was kept low (approximately 1.4 μJ/pulse) to prevent sample degradation.

Quantum mechanical calculations were performed with the Gaussian 03 program suite.[35] For all atoms except the central metal, the 6-31G(d)[36] basis set was used. For the central metals, the CEP (Stevens/Basch/Krauss ECP)[37−39] basis set was used. In this basis set, the core electrons are replaced with an effective core potential (ECP) to account for relativistic effects. The nonsubstituted metal−porphines were chosen as models in order to reduce calculation time. Each metal−porphine was first geometry-optimized with D_{4h} symmetry constraints using the B3LYP functional.[40−42] The symmetry constraints were considered to be justified as optimizations with and without constraints, resulting in very similar structures for both metalation states. The resulting D_{4h} optimized geometries were then used for time-dependent density functional theory (TD-DFT)[43−45] calculations of the vertical excited states using the same functional and basis sets as for the geometry optimizations.

Results

Steady-State Measurements. Figure 2 shows the absorption and emission spectra of the studied gold(III) porphyrins. They

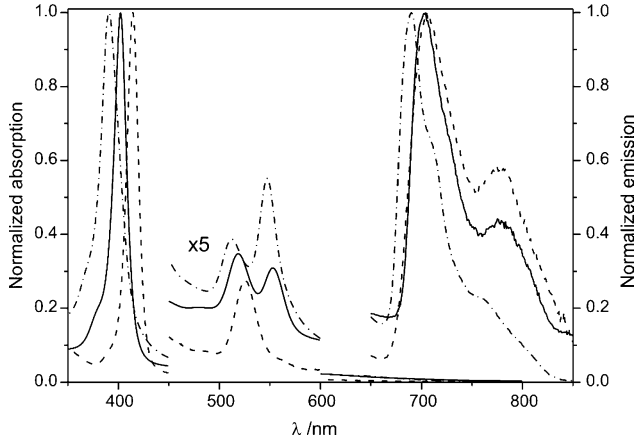

Figure 2. Absorption spectra (left) at room temperature and emission spectra (right) at 80 K for AuP (—), AuT(DtBP)P (- -), and AuOEP (- · -) in EPA. The excitation wavelengths were 518, 524, and 547 nm for AuP, AuT(DtBP)P, and AuOEP, respectively.

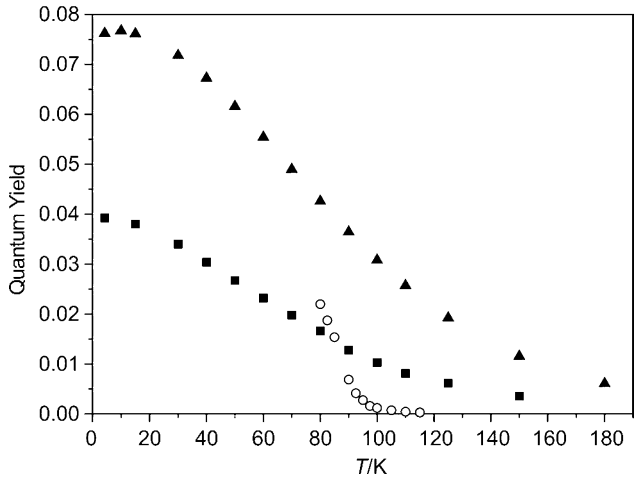

Figure 3. Quantum yields of phosphorescence vs temperature for AuP in PMMA (■) and EPA (○) and for AuT(DtBP)P in PMMA (▲). The excitation wavelengths were 518 and 524 nm for AuP and AuT(DtBP)P, respectively.

display the usual characteristics of hypso-porphyrins,[46] with the Soret or B-band around 400 nm and a Q-band centered at 530 nm. The studied compounds do not emit in fluid media but phosphoresce in *rigidified* media at low temperatures.

Figure 3 shows the quantum yield of phosphorescence as a function of temperature for AuP and AuT(DtBP)P in a PMMA matrix. In PMMA, the phosphorescence of all the studied compounds is virtually undetectable at temperatures above 200 K, but at lower temperatures the quantum yields increase, in a sigmoidal fashion, to level out at 4 K to a maximum value of about 8% and 4% for AuT(DtBP)P and AuP, respectively. In EPA, there is virtually no emission until the glass setting temperature (at around 95 K) is approached and the viscosity is increased. At lower temperature, there is a sharp increase in the phosphorescence quantum yield (Figure 3), probably caused by slower bimolecular deactivation due to the large increase in viscosity. Since we are primarily interested in the intrinsic photophysics of the gold porphyrins, and studying its variations over larger temperature intervals, we will mostly focus on the measurements done in PMMA since this media is a glass throughout the whole temperature range of interest, 4−300 K, and will efficiently prevent any bimolecular processes.

Time-Resolved Measurements. Transient absorption measurements at low temperatures show the two previously

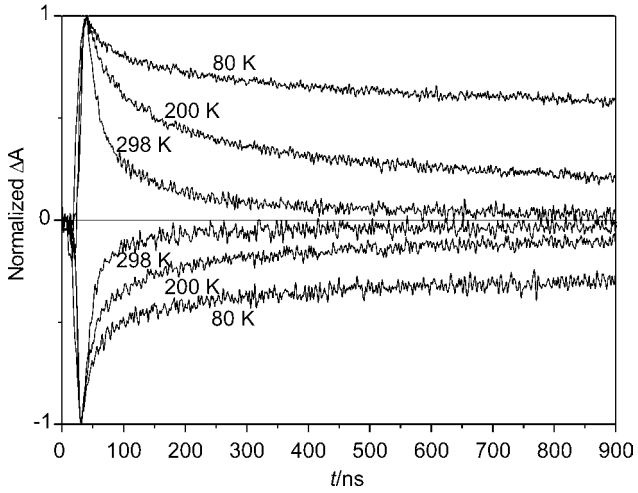

Figure 4. Transient absorption (positive), probed at 450 nm, and ground-state bleaching (negative), probed at 412 nm, of AuT(DtBP)P in PMMA at 298, 200, and 80 K. The excitation wavelength was 532 nm.

observed[6,7,10,12,13,27] lifetimes of about 10 and 100 μs at 80 K for AuT(DtBP)P in PMMA. However, measurements at higher time resolution reveal (Figure 4) an additional significant and short-lived component with a lifetime of about 20−50 ns. In EPA, this short lifetime (as well as the two longer lifetimes) is only observed between 80 and 140 K (not shown), because at higher temperatures the lifetimes become too short to detect with the experimental setup used. In PMMA, however, three lifetimes are observed for all studied gold(III) porphyrins in the entire temperature interval (4−300 K), and the short lifetime is approximately temperature-independent. The fact that all three lifetimes are present in EPA at temperatures when the solvent is still fluid (120−140 K) indicates that the phenomenon does not originate from the presence of different conformations of the molecules frozen in the solid matrix but is an inherent characteristic of gold(III) porphyrins. To identify the properties of the short-lived component, transient absorption measurements were performed at wavelengths where either the ground state (412 nm) or the excited state (450 nm) dominates the absorption. At room temperature, the fitting of both the transient absorption decay and the ground state recovery requires three exponential functions. At lower temperatures, though, the lifetimes of the short-lived and the two long-lived components deviate too much from each other, making it experimentally impossible to fit all three in one decay trace. This makes obtaining quantitative information (i.e., accurate rate constants) about the short-lived state difficult. However, it is possible to come to the following qualitative conclusions.

The observation of the same three lifetimes in the ground-state recovery and in the transient absorption decay indicates that all three excited states are independently coupled to the ground state. However, from a careful comparison of the decay traces in Figure 4, it can be seen that the relative contributions of the short-lived and the two long-lived states are not the same in the ground-state recovery as in the transient absorption decay. This is most obvious at low temperatures where the relative contribution of the short-lived component is clearly larger in the ground-state recovery (negative) than in the transient absorption decay (positive). This could either mean that the short-lived state has the same shape of its transient absorption spectrum as the two long-lived states but a smaller absorption coefficient or a different shape of its transient absorption spectrum. On one hand, if all species have the same shape of their transient absorption spectra, then no difference between

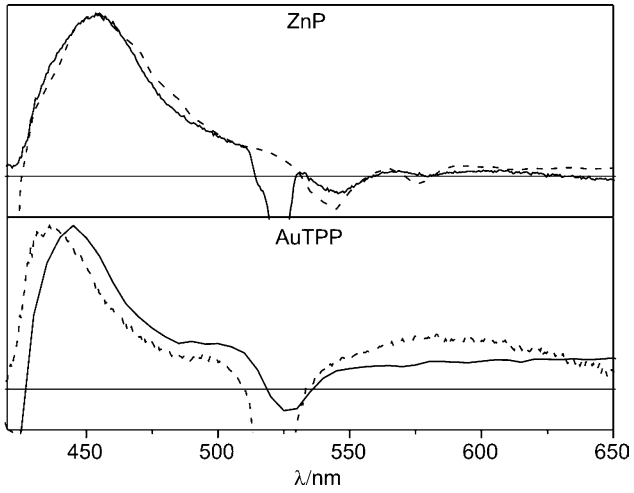

Figure 5. Transient absorption spectra of ZnP (top) at 1.5 ns in EPA (- -) and 100 ns in 2-MTHF at 150 K (—) and of AuT(DtBP)P (bottom) at 1.5 ns in EPA at room temperature (- -) and at 100 ns in EPA at 80 K (—).

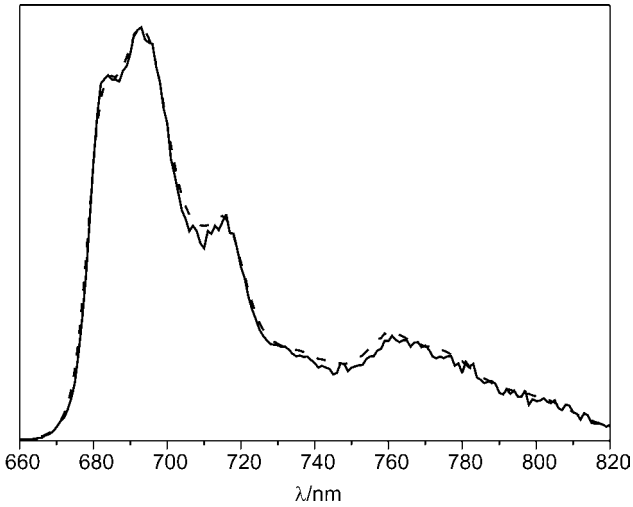

Figure 6. Steady-state emission spectrum (—) and the time-gated (10 μs—1.3 ms) emission spectrum (- -) of AuP in EPA at 80 K. The excitation wavelength was 518 nm.

spectra recorded at short and longer times is expected. If, on the other hand, the short-lived species have different shape of their transient absorption spectra, then a spectral evolution on the nanosecond time scale would be expected.

To distinguish between the two possibilities, transient absorption spectra recorded at two delay times are expected to be informative. The short-lived state dominates the transient absorption spectra at times shorter than 20 ns and the two long-lived states at times longer than 100 ns. Ideally, these spectra would be measured with the same experimental setup, but due to experimental difficulties with scattering and impurities the time resolution of our nanosecond setup was not good enough to record the transient spectrum of the short-lived species. The transient absorption spectrum of the initially formed species was therefore recorded with a pump—probe system having picosecond time resolution. For this measurement, room temperature and fluid media were necessary because in the highly focused laser beams the use of rigid media led to severe photodegradation of the solid samples. In addition, measurements of spectra for the long-lived species required high viscosity (glass) and low temperature. Since the measurements had to be done with different experimental setups for the two delay times, measurements were also performed on ZnP, a well-characterized porphyrin not expected to display spectral evolution in this time frame. Figure 5 (bottom) shows the transient absorption spectrum for AuT(DtBP)P after 1.5 ns at room temperature and after 100 ns (when the short-lived component has decayed) at 80 K. It can be seen that there is a spectral evolution between the two delay times, which gives strength to the earlier indication of different transient absorption spectral profiles of the short-lived and the two longer-lived transient states. It can also be seen in Figure 5 (top) that there is good general correlation between measurements performed on the two different setups for ZnP. Thus, the spectral evolution displayed for AuT(DtBP)P in the time window between the two measurements cannot be explained by experimental differences.

Having established that the short-lived component has a different transient absorption spectrum than the two long-lived components, resulting in a spectral evolution that takes place within the first 100 ns, we now turn to investigate the properties of the two remaining states. After the first 100 ns, there is no observed spectral evolution, which indicates that the two long-lived states have the same shape of their transient absorption spectra. Also, their relative contributions in transient absorption (probed at 450 nm) and the ground-state recovery (probed at 412 nm) are the same, indicating similar absorption coefficients of the two states. To further investigate the spectral properties of the emission from the two long-lived species, a time-gated phosphorescence spectrum of AuP in EPA at 80 K, collecting the emission between 10 μs and 1.3 ms, was compared to the steady-state spectrum. This comparison is displayed in Figure 6 and shows the invariance of the shape of the phosphorescence spectrum after time gating, which indicates that the two long-lived states have the same emission profile and thus are degenerate. The invariance of the phosphorescence spectrum together with the early spectral evolution of the transient absorption spectrum also suggests that the short-lived state is nonemissive.

A summary of the results from the time-resolved measurements is that the short-lived state is most probably populated with unit efficiency from the excited singlet state since deactivation of the singlet is very fast ($(240\ \text{fs})^{-1}$)[22] and it is most improbable that several processes operate in parallel on this time scale. If the short-lived state is populated from the excited singlet with unit efficiency, then there is no other possible route for populating the two long-lived states than from the short-lived state. The short-lived state is thus directly coupled to the ground state *and* to the two long-lived states.

Quantum Chemical Calculations. To gain insight into the character of the excited states, we investigated the differences between the two metalation states, ZnP and AuP, in a set of DFT calculations performed on the corresponding metal—porphines. As was the case in the time-resolved transient absorption study (see above), ZnP was used for comparison because of its regular and well-characterized photophysics. The resulting frontier orbitals of the geometry-optimized molecules are shown in Figure 7 and reveal important differences for AuP (left) relative to ZnP (right). The calculated frontier orbitals of ZnP are the normal highest occupied molecular orbitals (HOMOs) and lowest unoccupied molecular orbitals (LUMOs) of regular porphyrins,[46] but AuP has an orbital with pronounced $d_{x^2-y^2}$ character raised in energy, relative to ZnP, so that it becomes the LUMO of the system. This orbital ordering is different from earlier results from iterative extended Hückel (IEH)[27] and Xα multiple scattering[47] calculations, which predicted a higher energy for this orbital resulting in an orbital ordering with this metal-centered orbital *above* the ring-centered e_g orbitals. It

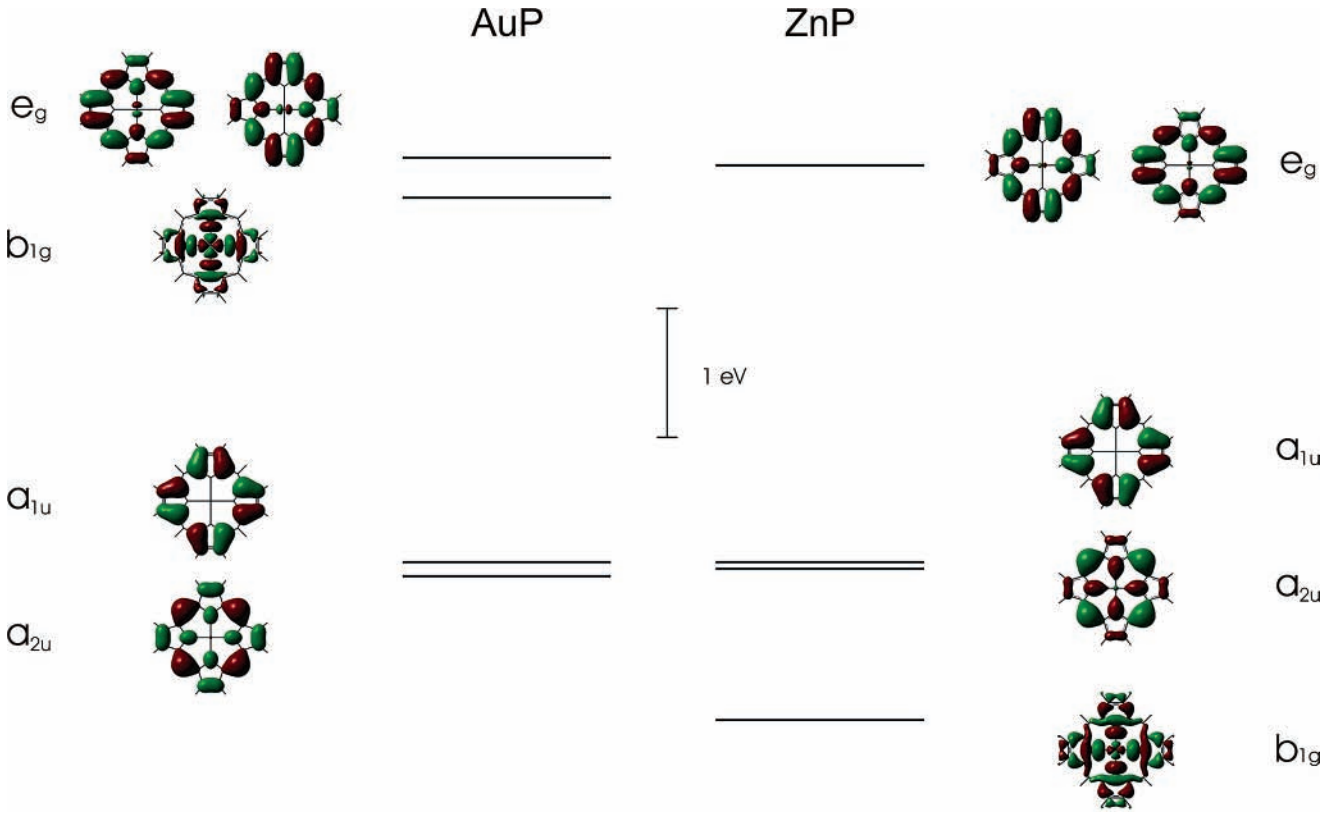

Figure 7. Frontier orbital diagram for gold(III) porphine (left) and zinc(II) porphine (right).

could be suspected that the orbital ordering might be sensitive to the substitution pattern of the porphyrin ring, but geometry optimization of gold(III) diphenyl-octamethyl-porphyrin did not change the orbital ordering and even lowered the energy of the metal-centered orbital. Our result, placing the metal-centered orbital below the unoccupied ring-centered orbitals, goes hand in hand with recent studies showing that the first reduction[25,26] as well as the accepting of an electron in electron-transfer reactions[2] is metal-centered in gold(III) porphyrins. To investigate the effects on the excited electronic states caused by the difference in orbital ordering between the two metalation states, a set of TD-DFT calculations were performed. This set of calculations, not surprisingly, resulted in several low-lying states with pronounced ligand-to-metal charge-transfer (LMCT) character for AuP (Table 1). Transition from the ground state to one of these is weakly allowed and has also been observed in experiments as a small shoulder between the Soret- and Q-bands.[27,28] It can bee seen from Table 1 that the TD-DFT calculations consistently overestimate the excitation energies for both AuP and ZnP with approximately 0.3 eV, but the energy separation between the Soret- and Q-bands is accurately described. Thus, so far, the calculations give results that are consistent with experimental observations. Having established that the calculations give results that can be verified by experiments, we now turn to the calculated differences between AuP and ZnP that are hard to directly detect experimentally. The most striking difference is that for AuP the two lowest excited singlet states are of LMCT character. For ZnP, however, the lowest excited singlet states are the normal ligand-localized states associated with the Q-band absorption. Thus, from the calculations, the different photophysics of AuP could be explained by the presence of LMCT states located between the lowest singlet and triplet states. The triplet versions of the low-lying CT states in AuP are nearly degenerate with the normal ligand-localized triplets.

TABLE 1: Calculated Vertical Excitation Energies and Oscillator Strengths (*f*) of Gold(III) and Zinc(II) Porphine[f]

	AuP		ZnP	
character	*E* (eV)	*f*	*E* (eV)	*f*
	Singlets			
E_u, B-band	3.52 (3.18)[a]	0.7062	3.54 (3.22)[c]	0.8907
A_{2u}, CT	3.39 (2.76)[b]	0.0001		
E_g, CT	3.05		3.43	
E_u, Q-band	2.53 (2.27)[a]	0.0038	2.44 (2.17)[c]	0.0023
B_{2u}, CT	2.02			
B_{1u}, CT	1.93			
	Triplets			
E_u	2.16		2.08	
B_{2u}, CT	1.92			
B_{1u}, CT	1.90			
E_u	1.88 (1.80)[d]		1.77 (1.72)[e]	

[a] Value for AuOEP in MMA (this study). [b] Value for AuT(DtBP)P from refs 27 and 28. [c] Value for ZnOEP vapor from ref 46. [d] Value from phosphorescence maximum of AuOEP in PMMA (this study). [e] Value for Zn−porphine from ref 49. [f] Experimental values (when available) are given in parentheses.

Also, if one compares the ground-state absorption spectra of AuP and ZnP (Figure 1S in the Supporting Information), then one can see clear differences that can be explained by the calculations. The absorption spectra of the two metalation states are very similar in that they have the same number of peaks with roughly the same relative intensity. The most obvious difference is that for AuP the absorption tails out into the far red of the spectrum whereas for ZnP the absorption decreases abruptly at the absorption edge. This might be explained by transition to the LMCT state between the B- and Q-bands and transitions to the formally forbidden LMCT states below the Q-band for AuP. For ZnP, these states are not present, and the porphyrin displays a normal absorption spectrum.

Solvent Polarity Dependence. To get experimental indications for the presence of a low-lying CT state, we studied AuT-

TABLE 2: Quantum Yield of Phosphorescence (Φ_p), the Lifetimes (τ), and Their Corresponding Preexponential Factors (α) from Transient Absorption Decays[b]

solvent		Φ_p	τ_1 (ns)	α_1 (%)	τ_2 (μs)	α_2 (%)	τ_3 (μs)	α_3 (%)
EPA	mp	0.0167	40	29	11	18	124	53
2-MTHF	lp	0.0086	48	64	3.7	25	83	11
toluene/MCH[a]	lp	0.0074	34	71	3.4	17	82	12

[a] A mixture of toluene/methyl cyclohexane, 1:6. [b] The presented data are for AuT(DtBP)P in more polar (mp) and less polar (lp) solvents at 80 K. The excitation wavelength was 532 nm.

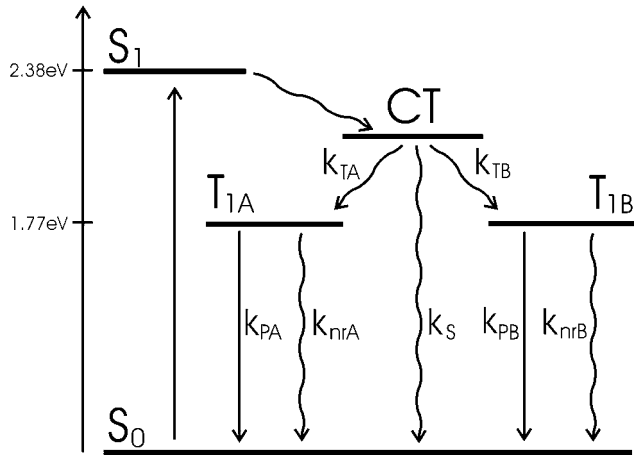

Figure 8. Proposed model for deactivation of excited gold(III) porphyrins.

(DtBP)P in different solvents (Table 2). When switching from more polar solvents to solvents of lower polarity, the energy of a CT state would be expected to increase more than the energy of the less polar triplet states. This would increase the CT−T_1 energy gap and lead to less formation of the triplets from the CT state and, hence, a larger contribution from the short-lived state in the ground-state recovery. The results show that in the more polar EPA the phosphorescence quantum yield and the relative contribution of the three components to the total transient absorption are clearly different from the other, less polar solvents (2-MTHF and a mixture of toluene and methylcyclohexane). The less polar solvents increase the contribution of the short-lived state to the decay and also decrease the phosphorescence quantum yield in the same proportion, again indicating that the short-lived state is nonemitting. The results from the solvent study, thus, suggest that the dark state has CT character.

Discussion

The results above give support for the model depicted in Figure 8, with the excited singlet state populating a dark CT state that in turn populates two degenerate triplet states in parallel. The two triplet states are subsequently deactivated to the ground state independently. The lowest excited singlet is only directly coupled to the CT state since the rate constant for depopulation of the excited singlet is very large, $(240\ \text{fs})^{-1}$ for AuP,[48] and it is improbable that another deactivating process (internal conversion to the ground state or intersystem crossing to the triplet manifold) operates in parallel on this time scale. The decay kinetics based on the proposed model were used to derive a method to fit the transient absorption decay data globally, as follows. The decay of the transient absorption, after the short-lived component has decayed, at a given temperature can be expressed as a sum of two exponential decays with

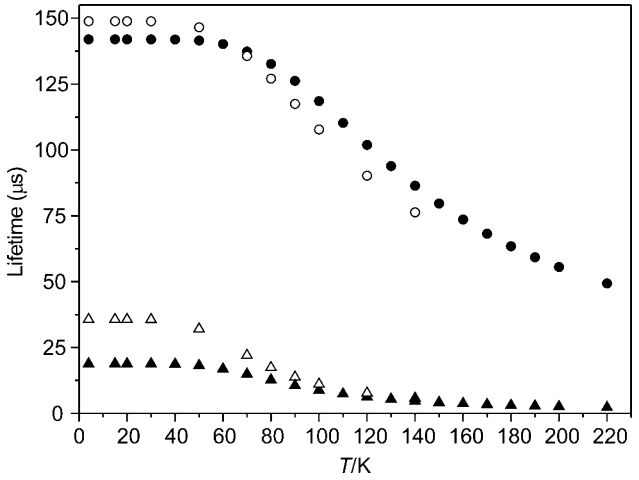

Figure 9. Lifetimes of the most long-lived (circles) and middle-lived (triangles) components for AuP (○ and △) and AuT(DtBP)P (● and ▲) from the global fitting procedure.

temperature-dependent rate constants (k_A,k_B) and preexponential factors (α_A,α_B)

$$\Delta A(t,T) = \alpha_A(T)\, e^{-tk_A(T)} + \alpha_B(T)\, e^{-tk_B(T)} \qquad (1)$$

The effect of temperature on the preexponential factors in eq 1 was not a priori settled, but instead the values were allowed to vary at all temperatures, and thus, the temperature variation was revealed from the fitting results. The temperature dependence of the rate constants was assumed to be described by Arrhenius type expressions, giving the rate of deactivation from the two triplets as a function of temperature as

$$k_A(T) = k_{PA} + A_A\, e^{(-E_{aA}/RT)} \quad k_B(T) = k_{PB} + A_B\, e^{(-E_{aB}/RT)} \qquad (2)$$

Here, k_{PA} and k_{PB} are the rate constants for phosphorescence, and E_{aA} and E_{aB} are the activation energies for nonradiative deactivation (intersystem crossing to the ground state) of states A and B, respectively. The parameters k_{PA}, A_A, E_{aA}, α_A, k_{PB}, A_B, E_{aB}, and α_B were varied to give as good a fit as possible of eq 1 to all of the individual decay traces in the whole temperature interval at the same time. This procedure gives a good fit to all of the individual decays, and the resulting lifetimes are within 10% of the ones attained when fitting the transient decays individually. The temperature intervals were 4−160 K for AuP and 4−220 K for AuT(DtBP)P, with a total of 11 and 22 decay traces in the global fitting procedures, respectively.

Figure 9 shows the lifetimes at different temperatures of the two long-lived components for AuP and AuT(DtBP)P in PMMA from the global fitting procedure. The lifetimes show similar temperature dependences as that of the phosphorescence quantum yield (Figure 3). The fitting procedure also yields the activation energies for nonradiative deactivation from the most long-lived (A) and middle-lived (B) states as $E_{aA} = 2.7$ kJ/mol and $E_{aB} = 2.5$ kJ/mol for AuP and $E_{aA} = 3.1$ kJ/mol and $E_{aB} = 3.7$ kJ/mol for AuT(DtBP)P.

As a check of the consistency of the model, it is possible to compare the results from the phosphorescence quantum yield measurements to the average relative populations (f_i) of the two emitting states. The average relative population of an emitting state, $f_i = \alpha_i\tau_i = \alpha_i k_i^{-1}$, should be proportional to the quantum yield of emission (Φ_i) from this state. For this relation to hold, it is important to note that the states have to be populated and depopulated independently. Figure 10 shows f as a function of

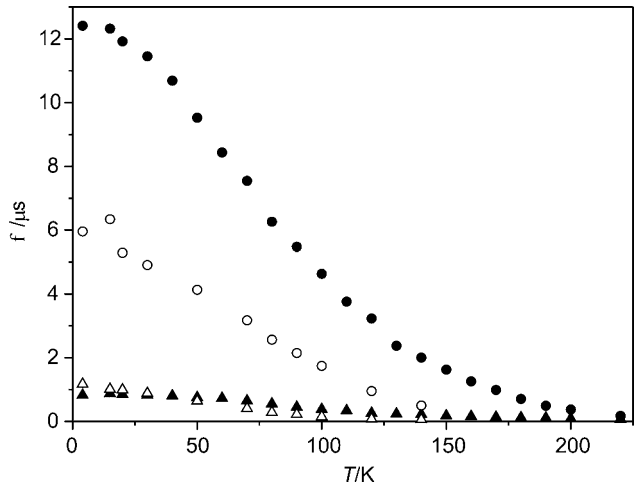

Figure 10. Average relative population of the most long-lived (circles) and middle-lived (triangles) components for AuP (○ and △) and AuT-(DtBP)P (● and ▲) from the global fitting procedure.

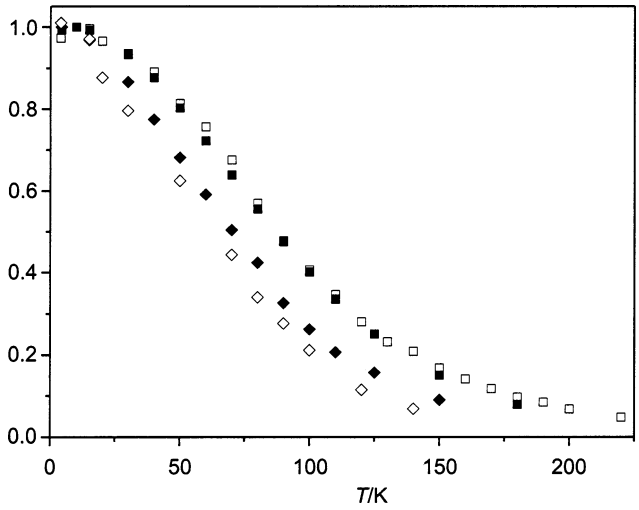

Figure 11. Quantum yields of phosphorescence (filled symbols) and the sums of the average relative populations ($f_A + f_B$) of the two long-lived components (open symbols) from the global fitting procedure for AuP (◆ and ◇) and AuT(DtBP)P (■ and □). The properties are normalized for comparison.

temperature of the most long-lived (f_A) and middle-lived (f_B) states, for AuP and AuT(DtBP)P in PMMA. The value of f gives an indication of the relative contribution to the total quantum yield from the individual states. It can be seen that the most long-lived state gives the largest contribution to the total quantum yield and that the temperature dependence is similar to that of the phosphorescence quantum yield (Figure 3). The difference in phosphorescence quantum yield between AuP and AuT(DtBP)P is also reflected in Figure 10 in that for AuT-(DtBP)P the sum of f_A and f_B is approximately twice as high as that for AuP, which is also the case for the phosphorescence quantum yields. This shows that the phosphorescence quantum yields of the two porphyrins are related in the same way to the average relative populations. It was previously established that the two emitting states have the same emission spectra (Figure 3), and thus the sum of f_A and f_B should be compared to the total steady-state phosphorescence quantum yield. Figure 11 shows the temperature dependence of the quantum yield of phosphorescence and of the sum of f_A and f_B, both normalized at 4 K. It can be seen that fitting the data from the time-resolved measurements according to the model with the global fitting procedure gives a very good correlation to the steady-state quantum yield for both AuP and AuT(DtBP)P, giving further strength to the proposed model.

TABLE 3: Quantum Yield of Phosphorescence and Rate Constants, Calculated According to Appendix A, with τ_{CT} Assumed to Have a Constant Value of 50 ns[a]

	AuT(DtBP)P		AuP	
	4 K	200 K	4 K	150 K
Φ_p (%)	8	0.55	4	0.35
k_S/s^{-1}	1.8×10^7	1.9×10^7	1.9×10^7	2×10^7
k_{TA}/s^{-1}	1.1×10^6	2.3×10^5	4.4×10^5	1×10^5
k_{TB}/s^{-1}	5.4×10^5	1.2×10^6	3.6×10^5	1.6×10^5
k_{nrA}/s^{-1}	0	1×10^4	0	7.4×10^3
k_{PA}/s^{-1}	7×10^3	7×10^3	6.7×10^3	6.7×10^3
k_{nrB}/s^{-1}	0	2.4×10^5	0	1.7×10^5
k_{PB}/s^{-1}	4.8×10^4	4.8×10^4	2.8×10^4	2.8×10^y

[a] See Figure 8 for details.

The good correlation between experiments and global fittings to the model gives strength to the assumption that the two triplet states decay in parallel with no or little interconversion in the temperature intervals given above. As the temperature increases above the interval though, the observed lifetimes become shorter than those predicted by the globally fitted parameters. This indicates thermal activation of additional deactivation processes that are not included in the model. Examples of such processes are the back reaction from the triplets to the CT state or interconversion between the triplets. It can be seen from the DFT calculations that to reach the lowest excited singlet state from the lowest triplet state in a stepwise fashion a thermal energy of about 230 K (0.02 eV) is required. This is in agreement with the finding that the simple model depicted in Figure 8 holds for temperatures below 200 K but fails at higher temperatures. The failure of the model at higher temperatures could then be explained by thermal back reaction to the lowest excited singlet state, which subsequently is deactivated to the ground state.

When making estimations of the rate constants given in Figure 8, one can use the fact that at 4 K the nonradiative processes from the triplet states are turned off. This can be seen in Figures 3 and 9 as a leveling out of the quantum yield of phosphorescence and the lifetimes, at lower temperatures, to a maximum value. The quantum yield of phosphorescence and a reasonable value of the lifetime of the short-lived component (50 ns) then yields the rate constants given in Table 3. To more easily see the temperature effect, the rate constants are calculated at two extreme temperatures, the lowest, 4 K, and near the limit where the phosphorescence quantum yield was too low to be detected, 150 and 200 K for AuP and AuT(DtBP)P, respectively. The rate constants are derived by solving the differential equations for the population of the states according to the model in combination with the phosphorescence quantum yield measurements as described more thoroughly in Appendix A. One can see from Table 3 that as the temperature is increased less of the triplet states are formed and the phosphorescence is also quenched by the temperature-dependent intersystem crossing processes. The attentive observer may note that the rate constants for formation of the two triplet states (k_{TA} and k_{TB}) decrease slightly with increasing temperature. This would indicate negative activation energies, but since the calculations were highly approximate we estimate this to be within the error of uncertainty.

Conclusions

We have investigated the photophysics of gold(III) porphyrins with steady-state and time-resolved spectroscopic methods as

well as DFT calculations. It was found that the deactivation of the excited gold(III) porphyrins can be described by the model presented in Figure 8, at low temperatures in rigid media. We have observed a short-lived state, with a lifetime of about 20−50 ns in rigid media, that is an intermediate between the first excited singlet state and the triplet manifold and acts as a gatekeeper state for formation of the triplets. We show, by calculations and solvent studies, that this short-lived state is of pronounced LMCT character with a small splitting between its singlet and triplet versions. Once the lowest triplets have been formed from this CT state, they are deactivated to the ground state in parallel, without any interconversion at temperatures below 200 K. Furthermore, as the temperature is raised, the triplets are deactivated by additional pathways, presumably through thermal excitations to the CT state.

Acknowledgment. This work was supported by grants from the Swedish Research Council, the Knut and Alice Wallenberg Foundation, and the Hasselblad Foundation.

Supporting Information Available: Comparison of the Q-band region of the absorption spectra of AuP and ZnP. This material is available free of charge via the Internet at http://pubs.acs.org.

Appendix A

The differential equations for the population of the states according to the model described in Figure 8, if one assumes that the CT state is formed immediately with a concentration of $[CT]_0$, can be written as

$$-\frac{d[CT(t)]}{dt} = [CT(t)](k_S + k_{TA} + k_{TB})$$

$$-\frac{d[T_{1A}(t)]}{dt} = [T_{1A}(t)](k_{nrA} + k_{PA}) - [CT(t)]k_{TA}$$

$$-\frac{d[T_{1B}(t)]}{dt} = [T_{1B}(t)](k_{nrB} + k_{PB}) - [CT(t)]k_{TB} \quad (1A)$$

Solving these equations leads to the following time dependence of the populations

$$[CT(t)] = [CT]_0\, e^{-(k_S+k_{TA}+k_{TB})t} = [CT]_0\, e^{-t/\tau_{CT}}$$

$$[T_{1A}(t)] = \frac{[CT]_0 k_{TA}(e^{-(k_{nrA}+k_{PA})t} - e^{-(k_S+k_{TA}+k_{TB})t})}{k_S + k_{TA} + k_{TB} - k_{nrA} - k_{PA}} = \frac{[CT]_0 k_{TA}(e^{-t/\tau_A} - e^{-t/\tau_{CT}})}{1/\tau_{CT} - 1/\tau_A}$$

$$[T_{1B}(t)] = \frac{[CT]_0 k_{TB}(e^{-(k_{nrB}+k_{PB})t} - e^{(k_S+k_{TA}+k_{TB})t})}{k_S + k_{TA} + k_{TB} - k_{nrB} - k_{PB}} = \frac{[CT]_0 k_{TB}(e^{-t/\tau_B} - e^{-t/\tau_{CT}})}{1/\tau_{CT} - 1/\tau_B} \quad (2A)$$

The relative concentration of the A and B states is then

$$\frac{[T_{1A}(t)]}{[T_{1B}(t)]} = \frac{k_{TA}(e^{-t/\tau_A} - e^{-t/\tau_{CT}})(1/\tau_{CT} - 1/\tau_B)}{k_{TB}(e^{-t/\tau_B} - e^{-t/\tau_{CT}})(1/\tau_{CT} - 1/\tau_A)} \quad (3A)$$

Equation 3A can be greatly simplified by using approximations based on the fact that the lifetime of the two long-lived states are about 1000 times larger than that of the short-lived state, i.e., $\tau_{CT} \ll \tau_{T1A} \approx \tau_{T1B}$.

(1) At intermediate times, when the short-lived state has decayed and the two long-lived states have just been formed, the two parentheses containing the exponentials can each be approximated by

$$(e^{-0} - e^{-\infty}) = 1$$

(2) The parentheses containing the lifetimes can be approximated by $\tau^{-1}_{CT} = k_{CT}$.

For the two long-lived states, this intermediate time is negligible and can be regarded as time zero, and thus the relative concentrations of the two states at intermediate times can be approximated by α_A/α_B, the preexponential factors from the global fitting procedure.

This reduces eq 3A to

$$\frac{\alpha_A}{\alpha_B} = \frac{k_{TA}}{k_{TB}} \quad (4A)$$

Equation 4A contains two unknowns, and thus we need another relationship between k_{TA} and k_{TB}. For this, we can turn to the phosphorescence quantum yield. The total quantum yield of phosphorescence from the two triplet states can be expressed in rate constants and lifetimes according to

$$\Phi_P = \Phi_{PA} + \Phi_{PB} = \frac{k_{TA}}{k_S + k_{TA} + k_{TB}} \frac{k_{PA}}{k_{nrA} + k_{PA}} + \frac{k_{TB}}{k_S + k_{TA} + k_{TB}} \frac{k_{PB}}{k_{nrB} + k_{PB}} = k_{TA}\tau_{CT} k_{PA}\tau_A + k_{TB}\tau_{CT} k_{PB}\tau_B \quad (5A)$$

In eq 5A, everything but k_{TA} and k_{TB} is known from the global fitting procedure, and thus if we combine eqs 4A and 5A we have enough information to estimate the rate constants k_{TA} and k_{TB} at different temperatures.

References and Notes

(1) Sundström, V.; Pullerits, T.; Van Grondelle, R. *J. Phys. Chem. B* **1999**, *103*, 2327.
(2) Fukuzumi, S.; Ohkubo, K.; E, W.; Ou, Z.; Shao, J.; Kadish, K. M.; Hutchison, J. A.; Ghiggino, K. P.; Sintic, P. J.; Crossley, M. J. *J. Am. Chem. Soc.* **2003**, *125*, 14984.
(3) Brun, A. M.; Harriman, A.; Heitz, V.; Sauvage, J. P. *J. Am. Chem. Soc.* **1991**, *113*, 8657.
(4) Chambron, J. C.; Harriman, A.; Heitz, V.; Sauvage, J. P. *J. Am. Chem. Soc.* **1993**, *115*, 7419.
(5) Chambron, J. C.; Harriman, A.; Heitz, V.; Sauvage, J. P. *J. Am. Chem. Soc.* **1993**, *115*, 6109.
(6) Dixon, I. M.; Collin, J. P.; Sauvage, J. P.; Barigelletti, F.; Flamigni, L. *Angew. Chem., Int. Ed.* **2000**, *39*, 1292.
(7) Dixon, I. M.; Collin, J. P.; Sauvage, J. P.; Flamigni, L. *Inorg. Chem.* **2001**, *40*, 5507.
(8) Flamigni, L.; Armaroli, N.; Barigelletti, F.; Chambron, J. C.; Sauvage, J. P.; Solladie, N. *New J. Chem.* **1999**, *23*, 1151.
(9) Flamigni, L.; Barigelletti, F.; Armaroli, N.; Collin, J. P.; Sauvage, J. P.; Williams, J. A. G. *Chem.—Eur. J.* **1998**, *4*, 1744.
(10) Flamigni, L.; Barigelletti, F.; Armaroli, N.; Ventura, B.; Collin, J. P.; Sauvage, J. P.; Williams, J. A. G. *Inorg. Chem.* **1999**, *38*, 661.
(11) Flamigni, L.; Dixon, I. M.; Collin, J. P.; Sauvage, J. P. *Chem. Commun.* **2000**, 2479.
(12) Flamigni, L.; Marconi, G.; Dixon, I. M.; Collin, J. P.; Sauvage, J. P. *J. Phys. Chem. B* **2002**, *106*, 6663.
(13) Harriman, A.; Heitz, V.; Ebersole, M.; Vanwilligen, H. *J. Phys. Chem.* **1994**, *98*, 4982.
(14) Harriman, A.; Odobel, F.; Sauvage, J. P. *J. Am. Chem. Soc.* **1994**, *116*, 5481.
(15) Harriman, A.; Odobel, F.; Sauvage, J. P. *J. Am. Chem. Soc.* **1995**, *117*, 9461.

(16) Linke, M.; Chambron, J. C.; Heitz, V.; Sauvage, J. P. *J. Am. Chem. Soc.* **1997**, *119*, 11329.
(17) Linke, M.; Chambron, S. C.; Heitz, V.; Sauvage, S. P.; Encinas, S.; Barigelletti, F.; Flamigni, L. *J. Am. Chem. Soc.* **2000**, *122*, 11834.
(18) Segawa, H.; Takehara, C.; Honda, K.; Shimidzu, T.; Asahi, T.; Mataga, N. *J. Phys. Chem.* **1992**, *96*, 503.
(19) Yeow, E. K. L.; Sintic, P. J.; Cabral, N. M.; Reek, J. N. H.; Crossley, M. J.; Ghiggino, K. P. *Phys. Chem. Chem. Phys.* **2000**, *2*, 4281.
(20) Kilså, K.; Kajanus, J.; Macpherson, A. N.; Mårtensson, J.; Albinsson, B. *J. Am. Chem. Soc.* **2001**, *123*, 3069.
(21) Pettersson, K.; Kilså, K.; Mårtensson, J.; Albinsson, B. *J. Am. Chem. Soc.* **2004**, *126*, 6710.
(22) Andréasson, J.; Kodis, G.; Ljungdahl, T.; Moore, A. L.; Moore, T. A.; Gust, D.; Mårtensson, J.; Albinsson, B. *J. Phys. Chem. A* **2003**, *107*, 8825.
(23) Shimidzu, T.; Segawa, H.; Iyoda, T.; Honda, K. *J. Chem. Soc., Faraday Trans. 2* **1987**, *83*, 2191.
(24) Tyulyaeva, E. Y.; Lomova, T. N. *Russ. J. Coord. Chem.* **2001**, *27*, 433.
(25) Ou, Z. P.; Kadish, K. M.; Wenbo, E.; Shao, J. G.; Sintic, P. J.; Ohkubo, K.; Fukuzumi, S.; Crossley, M. J. *Inorg. Chem.* **2004**, *43*, 2078.
(26) Kadish, K. M.; Wenbo, E.; Ou, Z. P.; Shao, J. G.; Sintic, P. J.; Ohkubo, K.; Fukuzumi, S.; Crossley, M. J. *Chem. Commun.* **2002**, 356.
(27) Antipas, A.; Dolphin, D.; Gouterman, M.; Johnson, E. C. *J. Am. Chem. Soc.* **1978**, *100*, 7705.
(28) Abou-Gamra, Z.; Harriman, A.; Neta, P. *J. Chem. Soc., Faraday Trans. 2* **1986**, *82*, 2337.
(29) Ding, H.; Dvornikov, A. S.; Straub, K. D.; Rentzepis, P. M. *Proc. SPIE-Int. Soc. Opt. Eng.* **1994**, *2137*, 581.
(30) Kilså, K.; Kajanus, J.; Macpherson, A. N.; Mårtensson, J.; Albinsson, B. *J. Am. Chem. Soc.* **2001**, *123*, 3069.
(31) Chambron, J. C.; Heitz, V.; Sauvage, J. P. *New J. Chem.* **1997**, *21*, 237.
(32) Rothemund, P.; Menotti, A. R. *J. Am. Chem. Soc.* **1948**, *70*, 1808.
(33) Patrick, T. B.; Disher, J. M.; Probst, W. J. *J. Org. Chem.* **1972**, *37*, 4467.
(34) Lindsey, J. S.; Wagner, R. W. *J. Org. Chem.* **1989**, *54*, 828.
(35) Frisch, M. J.; Trucks, G. W.; Schlegel, H. B.; Scuseria, G. E.; Robb, M. A.; Cheeseman, J. R.; Montgomery, J. A., Jr.; Vreven, T.; Kudin, K. N.; Burant, J. C.; Millam, J. M.; Iyengar, S. S.; Tomasi, J.; Barone, V.; Mennucci, B.; Cossi, M.; Scalmani, G.; Rega, N.; Petersson, G. A.; Nakatsuji, H.; Hada, M.; Ehara, M.; Toyota, K.; Fukuda, R.; Hasegawa, J.; Ishida, M.; Nakajima, T.; Honda, Y.; Kitao, O.; Nakai, H.; Klene, M.; Li, X.; Knox, J. E.; Hratchian, H. P.; Cross, J. B.; Adamo, C.; Jaramillo, J.; Gomperts, R.; Stratmann, R. E.; Yazyev, O.; Austin, A. J.; Cammi, R.; Pomelli, C.; Ochterski, J. W.; Ayala, P. Y.; Morokuma, K.; Voth, G. A.; Salvador, P.; Dannenberg, J. J.; Zakrzewski, V. G.; Dapprich, S.; Daniels, A. D.; Strain, M. C.; Farkas, O.; Malick, D. K.; Rabuck, A. D.; Raghavachari, K.; Foresman, J. B.; Ortiz, J. V.; Cui, Q.; Baboul, A. G.; Clifford, S.; Cioslowski, J.; Stefanov, B. B.; Liu, G.; Liashenko, A.; Piskorz, P.; Komaromi, I.; Martin, R. L.; Fox, D. J.; Keith, T.; Al-Laham, M. A.; Peng, C. Y.; Nanayakkara, A.; Challacombe, M.; Gill, P. M. W.; Johnson, B.; Chen, W.; Wong, M. W.; Gonzalez, C.; Pople, J. A. *Gaussian 03*, revision B.05; Gaussian, Inc.: Pittsburgh, PA, 2003.
(36) Ditchfield, R.; Hehre, W. J.; Pople, J. A. *J. Chem. Phys.* **1971**, *54*, 724.
(37) Cundari, T. R.; Stevens, W. J. *J. Chem. Phys.* **1993**, *98*, 5555.
(38) Stevens, W. J.; Basch, H.; Krauss, M. *J. Chem. Phys.* **1984**, *81*, 6026.
(39) Stevens, W. J.; Krauss, M.; Basch, H.; Jasien, P. G. *Can. J. Chem.* **1992**, *70*, 612.
(40) Becke, A. D. *J. Chem. Phys.* **1993**, *98*, 5648.
(41) Lee, C.; Yang, W.; Parr, R. G. *Phys. Rev. B: Condens. Matter Mater. Phys.* **1988**, *37*, 785.
(42) Vosko, S. H.; Wilk, L.; Nusair, M. *Can. J. Phys.* **1980**, *58*, 1200.
(43) Bauernschmitt, R.; Ahlrichs, R. *Chem. Phys. Lett.* **1996**, *256*, 454.
(44) Casida, M. E.; Jamorski, C.; Casida, K. C.; Salahub, D. R. *J. Chem. Phys.* **1998**, *108*, 4439.
(45) Stratmann, R. E.; Scuseria, G. E.; Frisch, M. J. *J. Chem. Phys.* **1998**, *109*, 8218.
(46) Gouterman, M. *Optical Spectra and Electronic Structure of Porphyrins and Related Rings*; Academic Press: New York, 1978; Vol. III.
(47) Sontum, S. F.; Case, D. A. *J. Phys. Chem.* **1982**, *86*, 1596.
(48) Andréasson, J.; Kodis, G.; Lin, S.; Moore, A. L.; Moore, T. A.; Gust, D.; Mårtensson, J.; Albinsson, B. *Photochem. Photobiol.* **2002**, *76*, 47.
(49) Murov, S. L., I. C.; Hug, G. L. *Handbook of Photochemistry*, 2nd ed.; Marcel Dekker: New York, 1993.